Thermodynamics of Core Hydrophobicity and Packing in the Hyperthermophile Proteins Sac7d and Sso7d†

Andrew T. Clark, Bradford S. McCrary, Stephen P. Edmondson,* and John W. Shriver*

Laboratory for Structural Biology, Departments of Chemistry and Biological Sciences, Graduate Program in Biotechnology and Bioengineering, University of Alabama in Huntsville, Huntsville, Alabama 35899

Received October 8, 2003; Revised Manuscript Received January 14, 2004

ABSTRACT: The influence of core hydrophobicity and packing on the structure and stability of the hyperthermophile proteins Sac7d and Sso7d have been studied by calorimetry, circular dichroism, and NMR. Valine 30 is positioned in Sac7d to allow a cavity-filling Val → Ile substitution which occurs naturally in the homologous more thermostable Sso7d. The cavity-filling mutation in Sac7d has been characterized and compared to the reciprocal Ile → Val mutation in Sso7d. A detailed analysis of the stability of the proteins was obtained by globally fitting the variation of DSC parameters and circular dichroism intensities as a function of temperature (0−100 °C), salt (0−0.3 M), and pH (0−8). A global analysis over such a range of conditions permitted an unusually precise measure of the thermodynamic parameters, as well as the separation of the thermodynamics of the intrinsic unfolding reaction from the linked effects of protonation and chloride binding associated with acid-induced folding. The results indicate differences in the energetics of unfolding Sac7d and Sso7d that would not be apparent from an analysis of DSC data alone using conventional methods. The sign and magnitude of the changes in ΔG, ΔH, $T\Delta S$, and ΔC_P of unfolding resulting from core Ile/Val substitutions in the two proteins were consistent with differences in hydrophobicity of Val and Ile and negligible changes in packing (van der Waals) interactions. The benefit of increased hydrophobicity of the core increased with temperature, with maximal effect around 116 °C. Increased hydrophobicity of the core achieved not only an increase in the free energy of unfolding, but also a lateral shift of the temperature of maximal stability to higher temperature.

The enhanced stability of thermophile proteins has been attributed to a number of factors based on comparisons of sequence and structural data (*1*−*18*). Some of the most common correlations have been increased ion pairs, greater hydrophobicity, and tighter packing of the core. Statistical evidence against the importance of packing in enhancing the stability of hyperthermophile proteins has been presented (*19*, *20*). Haney et al. (*21*) compared the sequence data available for homologous mesophile and thermophile proteins (115 total) and concluded that thermophile proteins have higher amino acid volumes, greater hydrophobicity, more charged residues, and fewer uncharged polar residues. In a recent study of homologous mesophile and thermophile proteins, differences in the number of cavities, hydrogen bonds, ion pairs, secondary structure, surface areas, and amino acid composition were correlated with growth temperature of the organism from which the proteins were isolated, and although statistical measures were used to document the reliability of differences between mesophile and thermophile homologues, the most notable observation was the high variability of the data and the lack of an overwhelming correlation (*22*). These data indicate that there is no unique factor responsible for enhanced stability, and it may be difficult to unambiguously explain the stability of thermophile proteins from the average behavior of a large sampling of structures and sequences. Any of the fundamental forces that stabilize proteins could be possible targets for optimization in thermophiles, and the ones used in a specific protein are most likely dependent on the protein fold and function. A more detailed understanding of thermophile protein stability will require knowledge of the thermodynamics of selected specific proteins and interactions.

Very little thermodynamic data are available to quantitatively describe either the global stability of thermophile proteins or the importance of specific interactions. Differences between the thermodynamic parameters describing the stability of thermophile and mesophile proteins have been recently compared (*23*, *24*), and the limited data collected to date indicates that thermophile protein stability is accomplished by an overall increase in the ΔG of unfolding, i.e., a vertical displacement of the protein stability curve (ΔG vs T). It was noted that mesophile proteins have an average temperature of maximal stability around 10 °C, but the range is large (−30 to 50 °C) and very much dependent on the accuracy of the ΔC_P for folding. The small amount of available data indicates that the average temperature of maximal stability for thermophile proteins is probably higher (around 35 °C) (*23*), i.e., not only is the stability curve shifted vertically but also laterally to higher temperature. The structural factors responsible for this are not understood.

† This work was supported by Grant GM49686 from the National Institutes of Health to J.W.S. and S.P.E.

* To whom correspondence should be addressed: John W. Shriver, Department of Chemistry, Materials Science Building, John Wright Drive, University of Alabama in Huntsville, Huntsville, AL 35899. Phone: 256-824-2477. Fax: 256-824-6349. E-mail: shriverj@uah.edu, edmonds@uah.edu.

10.1021/bi0358263 CCC: $27.50
Published on Web 02/18/2004

There have been a number of studies devoted to quantifying and distinguishing the contributions of hydrophobicity and packing (van der Waals interactions) to protein stability. Protein cores are preferentially hydrophobic (*25*−*27*), and optimal packing of the core should lead to extensive stabilizing van der Waals interactions (*28*−*31*). Some proteins are better packed than others. Almost any core modification in *Staphylococcal* nuclease was shown to be detrimental, even when the substitution involved essentially no change in hydrophobicity (e.g., Ile/Leu substitutions) (*32*). Early attempts to increase stability by filling cavities with more hydrophobic residues in the core of T4 lysozyme were shown to perturb the structure resulting in destabilization due to steric interactions (strain) (*33*). In RNase HI, however, cavity-filling mutations could be used to increase the T_m of the protein (*34*). Cavity-filling mutations in the R2 subdomain of c-Myb (such as V103I) also increased the stability significantly (*35*). Interestingly, increased stability can be coupled to increased packing density even if the enhanced stability is the result of surface residue substitutions (*36*). A number of *cavity-creating* studies have been published that generally demonstrate a loss in stability (*37*−*46*). In many of these systems, changes in the thermodynamic parameters other than ΔG are not consistent with a change in hydrophobicity alone, and loss of van der Waals interactions appears to be a dominant factor. However, in many of these the focus was on measurements of changes in ΔG of unfolding because of the difficulties in making precise measurements of ΔC_P. An assessment of the contributions of packing and hydrophobicity to protein stability requires an accurate and precise measure of changes in not only ΔG, but also ΔH, ΔS, and ΔC_P resulting from core substitutions. One of the goals of the work presented here is to define the limits of such measurements with extensive calorimetric as well as spectroscopic data.

Sac7d is a small protein (7.6 kDa) from the Archaea *Sulfolobus acidocaldarius* that unfolds reversibly with a T_m of 90.7 °C at pH 7 (*47*). The protein is globular and contains no disulfide or metal cofactors. Surprisingly, the NMR solution structure of the protein indicates that the core is not optimally packed (*48*). A cavity in the core of Sac7d should accommodate a Val 30 → Ile 30 substitution without significant modification of the structure. Indeed, this substitution occurs naturally in Sso7d, a homologous protein from the more thermophilic *Sulfolobus solfataricus* which has a T_m of approximately 99 °C at pH 7 (*49*). We have made the Sac7d V30I[1] and Sso7d I30V mutants and characterized the stabilities of Sac7d, Sso7d, and the two mutants using a multidimensional linkage analysis of the variation of CD spectral intensities and DSC data as a function of pH (0−8), salt (0−0.3 M), and temperature (0−130 °C). The thermodynamic data indicate that increased hydrophobicity of the core accounts for a significant portion of the increased stability of Sso7d relative to Sac7d. The data also demonstrate that the advantage of increased hydrophobicity of the core increases with temperature.

MATERIALS AND METHODS

Materials. Inorganic salts and buffers were obtained from Sigma Chemical Co. (St. Louis, MO). Recombinant Sac7d was prepared using a pET-3b expression vector construct in *Escherichia coli* (BL21 (DE3) pLysS) (*50*). Sso7d, Sac7d V30I, and Sso7d I30V were generated by site-directed mutagenesis of the Sac7d gene using the Transformer kit of Clontech (Palo Alto, CA). Protein concentrations were determined spectrophotometrically using the experimentally determined extinction coefficients for Sac7d and Sso7d (*50*). The extinction coefficients for Sac7d V30I and Sso7d I30V were assumed to be identical to Sac7d and Sso7d, respectively.

NMR. ^{1}H,^{15}N HSQC spectra were collected on 2.5 mM protein samples in 0.7 mL of 90% H_2O/10% D_2O at 30 °C using Varian INOVA 500 and 800 MHz NMR spectrometers with gradient selection of the ^{15}N magnetization and minimal perturbation of the water (*51*, *52*). ^{1}H chemical shifts were referenced to internal DSS, and the ^{15}N chemical shifts were calculated from the relative frequencies (Ξ) (*53*) of DSS (^{1}H) and liquid ammonia (^{15}N). V30I HSQC spectral peak assignments were easily made by comparison to the Sac7d HSQC assignments (*54*) due to negligible differences in the two spectra. Sso7d and I30V ^{1}H,^{15}N HSQC spectral assignments were obtained using a combination of 3D NOESY-HSQC and TOCSY-HSQC data (*52*) and previously obtained ^{1}H NMR assignments (*48*). Assignments have been deposited in the BioMagResBank (www.bmrb.wisc.edu) (accession numbers: Sac7d, 5905; V30I, 5908; Sso7d, 5909; I30V, 5910).

Differential Scanning Calorimetry (DSC). DSC was performed on Calorimetry Sciences Nano II DSC and MicroCal Extended Range VP-DSC calorimeters as previously described (*47*). Protein samples (approximately 1 mg/mL) were typically dialyzed overnight against approximately a 1000-fold excess of the appropriate buffer. Scans of degassed samples were routinely performed at 1 deg/min from 0 to 130 °C on the Nano II, and 1.5 deg/min from 5 to 125 °C on the VP-DSC. Baseline subtraction, concentration and scan rate normalization, and excess heat capacity analysis were performed using both software supplied by the manufacturers of the instruments and in-house software described previously (*47*, *55*) to obtain calorimetric and van't Hoff enthalpies as well as T_m. The reversibility of thermal unfolding was demonstrated by repetitive scans on the same sample.

Circular Dichroism Spectroscopy (CD). CD spectra were collected as described (*47*) with an AVIV 62DS spectropolarimeter with temperature maintained by a computer controlled thermoelectric unit. Variable temperature data were collected in 1-cm path length cuvettes. Thermal unfolding was typically monitored at 205 nm to obtain maximal signal-to-noise levels. Lower wavelengths proved to be inappropriate at low pH and high temperature due to increased absorbance of chloride.

Potential Energy Calculations. Potential energy calculations were performed using AMBER as described previously (*56*).

[1] Abbreviations: CD, circular dichroism; DSC, differential scanning calorimetry; NMR, nuclear magnetic resonance; V30I, the valine 30 to isoleucine 30 mutant of Sac7d; I30V, the isoleucine 30 to valine 30 mutant of Sso7d; ΔE, change in ΔH, ΔS, or ΔG with unfolding; $\Delta\Delta E$, change in ΔE as a result of an amino acid substitution; ΔC_P, change in heat capacity upon unfolding; T_m, midpoint temperature of a thermal unfolding transition; $\Delta H(T_m)$, change in enthalpy at the T_m; $\Delta S(T_m)$, change in entropy at the T_m.

Global Linkage Analysis. Circular dichroism spectral intensities and DSC stability parameters as a function of temperature, pH, and salt concentration were fit globally by nonlinear regression to a model in which protein folding is linked to changes in two chloride binding reactions and two protonation reactions as described below. The following data sets were fit simultaneously: (i) the pH dependence of the unfolding T_m (pH 0−8, about 25 data points) obtained by DSC at 0.3 M KCl ("high salt") (Figure 4), (ii) the variation of ΔH vs T_m (about 25 data points) obtained by DSC at high salt (Figure 5), and (iii) a series (8−12, 100 data points each) of CD thermal melts (Figure 6) as a function of pH in the absence of added salt ("low salt"), (iv) variation of the extent of unfolding with pH (pH 0−8, 15 to 30 data points) obtained from CD at 20 °C and low salt (Figure 6), and (v) for Sac7d, variation of extent of folding with salt concentration followed by CD (10−20 data points) at 25 °C and pH 2. The combined data sets for each protein typically contained a total of approximately 1100 data points. Chloride concentrations were converted to activities using the parametric equations of Pitzer (*57*). The sum of the squares of the residuals for each data set were weighted by the root-mean-square noise levels of the respective data sets. Parameter optimization was accomplished by iteratively applying adaptive grid refinement global optimization (Loehle Enterprises, Naperville, IL), grid search (*58*), and simplex optimization (*59*) until no further improvement of the reduced χ^2 was obtainable. Adaptive grid refinement has the advantage of locating multiple minima in a χ^2 surface and contracting a grid around each simultaneously. No evidence of multiple minima was obtained in the fitting of the data.

A model that links two ionization and two ligand binding reactions to protein folding contains at least 19 independent reactions (Figure 7), each of which is characterized by three independent thermodynamic parameters: an equilibrium constant (or equivalently a temperature where the equilibrium constant is one (i.e., a T_m)), ΔH, and ΔC_P. Even with the large amount of data available here, nonlinear regression with such a model is severely underdetermined. However, a systematic investigation of the sensitivity of the energetics of folding on individual parameters identified those parameters that are well defined by the data (*55*). In addition, reasonable limits can be placed on many of the parameters, and a number of parameters could be reliably fixed to literature values, e.g., the heats and heat capacities associated with protonation of carboxyl groups. The number of parameters was therefore reduced to 11: the ΔC_P of the intrinsic unfolding reaction, pK_u for the carboxyls in the unfolded protein which are affected by folding at low and high salt, pK_n for the same carboxyls in the native folded protein at low and high salt, pK_1 for these carboxyls in the folded protein with bound chloride at low and high salt, two chloride binding constants at low salt (K_{Cl} and K'_{Cl}), a single chloride binding constant at high salt (K_{Cl}), and the enthalpy and heat capacity of chloride binding.

The extent to which the 11 model parameters could be defined by the experimental data was determined by (i) statistical measures of the precision defined by variation of the parameters required to increase the reduced χ^2 by 1 (*58*), and (ii) investigating the errors in fitting simulated data sets, i.e., data created with known "target" parameters. The synthetic data sets contained the same number of data points over the same temperature, pH, and salt concentration ranges as the experimental data and Gaussian distributed noise with a standard deviation defined by that observed experimentally. Starting values for the parameters to initiate the regression were chosen to be experimentally reasonable, e.g., a ΔC_P initially defined by the Kirchhoff plot of ΔH vs T_m, a weak chloride binding constant, a small enthalpy and change in heat capacity associated with chloride binding, and p*K*'s of carboxyl groups in the vicinity of 4.0. The results indicated that 10 of the 11 parameters were well defined by data that resembled that observed for Sac7d (Supporting Information), and only the heat of anion binding was not well defined. It should be stressed that inclusion of more than two carboxyl ionizations (although not required by the data) would permit an increase in the unusually low p*K*'s of the carboxyl groups in the folded protein.

The ability to fit synthetic data similar to that observed for Sso7d was also investigated (i.e., data representing a protein with higher stability (including a higher T_m) and therefore demonstrating less effect of lower pH on the extent of unfolding). The results demonstrated that the agreement between the fitted and target values of the 11 parameters was generally quite good (Supporting Information). However, the higher protein stability in this example resulted in less of a change in the level of unfolding induced by changes in ionization and chloride binding, and therefore the precision with which associated parameters were defined was not as great as observed with synthetic Sac7d data. Interestingly, the precision for these parameters obtained by fitting experimental Sso7d and I30V data was better (see below).

Error Analysis. The precision[2] in measuring T_m was estimated from repeated DSC measurements under the same conditions. The precision in measuring ΔH was determined by the standard deviation of the distribution of residuals in Kirchhoff plots. The precision of the thermodynamic parameters fit in the global analysis was determined by the variation required to increase the reduced χ^2 of the fit by 1 (*58*). A mapping of the χ^2 surface by varying each parameter demonstrated that in some cases the depth of the minimum in the reduced χ^2 surface in that parameter space was less than one, and an upper and/or lower limit for such parameters could not be defined. In such cases, the precision limit is reported as infinite, indicating a lack of definition of the parameter by the data (e.g., the lower limit for pK_n).

An accurate and precise measure of the ΔC_P of unfolding is notoriously difficult to obtain (*60*−*62*). Errors in ΔC_P are commonly estimated to be on the order of 5−10% when determined with the Kirchhoff relation, i.e., $\partial\Delta H/\partial T_m$ (*63*). With more than 25 ΔH vs T_m pairs measured for each protein, we observed an error in ΔC_P from a Kirchhoff plot at the lower end of this range, i.e., around 5%. A global fitting of more than 40-fold more data points (>1000) resulted in significantly lower errors defined by the variation of χ^2. To err on the conservative side, we have applied the largest error observed in ΔC_P (for Sso7d) to all four proteins, i.e., ±19 cal/deg·mol (2.5%).

The temperature dependence of ΔG, ΔH, and ΔS was calculated using T_m, $\Delta H(T_m)$, and ΔC_P with the following

[2] Precision measures the reproducibility of a measurement. Accuracy measures the agreement between the experimentally measured and actual values (*58*).

equations:

$$\Delta H = \Delta H(T_m) + \Delta C_p(T - T_m) \quad (1)$$

$$\Delta S = \Delta S(T_m) + \Delta C_p \ln(T/T_m) \quad (2)$$

$$\Delta G = \Delta H\left(1 - \frac{T}{T_m}\right) + \Delta C_p\left(T - T_m - T\ln\left(\frac{T}{T_m}\right)\right) \quad (3)$$

where $\Delta S(T_m) = \Delta H(T_m)/T_m$. The errors in ΔH, ΔS, and ΔG were defined by the square root of the respective variances calculated using the following equations obtained from eqs 1−3 with standard propagation of error methods and assuming negligible covariances (*58*):

$$\sigma^2_{\Delta H} = \sigma^2_{H(T_m)} + \sigma^2_{\Delta C_p}(T - T_m)^2 + \sigma^2_{T_m}\Delta C_p^2 \quad (4)$$

$$\sigma^2_{\Delta S} = \sigma^2_{\Delta S(T_m)} + \sigma^2_{\Delta C_p}\left(\ln\frac{T}{T_m}\right)^2 + \sigma^2_{T_m}\left(\frac{\Delta C_p}{T_m}\right)^2 \quad (5)$$

$$\sigma^2_{\Delta G} = \sigma^2_{\Delta H}\left(1 - \frac{T}{T_m}\right)^2 + \sigma^2_{\Delta C_p}\left(T - T_m - T\ln\frac{T}{T_m}\right)^2 + \sigma_{T}m^2\left(\Delta C_p\left(\frac{T}{T_m} - 1\right) + \Delta H\frac{T}{T_m^2}\right)^2 \quad (6)$$

Errors in $\Delta\Delta E$ values were defined by the square root of the variance in $\Delta\Delta E$ given by

$$\sigma^2_{\Delta\Delta E} = \sigma^2_{\Delta E(1)} + \sigma^2_{\Delta E(2)} \quad (7)$$

The accuracy[2] of fitted parameters was investigated with simulated test data sets created with known "target" parameters, and comparison of known and fitted values. Simulated test data were created with random Gaussian distributed noise with a standard deviation equal to that observed in the corresponding experimental data. The accuracy of ΔG, ΔH, and $T\Delta S$ derived from the global linkage model was determined by the deviation of the values calculated using eqs 1−3 with parameters used for simulating test data (with noise) compared to values calculated with the fitted parameters.

The accuracy of the overall free energy of unfolding, ΔG_{unf}, which includes the intrinsic unfolding energy as well as those of ionization and ion binding, was investigated by comparing fitted free energy surfaces with the "true" surface calculated from the target parameters used to simulate the data. The two surfaces were in agreement to within 0.1 kcal/mol over most of the range of variables investigated here (Supporting Information). This indicates that the minimal model (although certainly oversimplified) was capable of accurately defining (fitting) the unfolding free energy surface.

RESULTS

Valine 30 of Sac7d is in the center of a three-stranded β-sheet, with the side chain inserted into the hydrophobic core (*48*) (Figure 1). It is adjacent to an internal cavity bounded by V30, A50, L55, L58, and the hydrophobic portions of the E47 and R25 side chains (Figure 2). The cavity is of sufficient size to accommodate the substitution of isoleucine for V30. The V30 side chain configuration about the C_α−C_β bond is g^+ with the C_βH proton trans to the C_αH. This is the lowest energy conformer, and a V30I substitution would be permitted without requiring rotomer redistribution. Potential energy calculations using AMBER indicated that the small-to-large Val → Ile substitution does not lead to steric interference or van der Waals overlap and can be accommodated with minimal perturbation of the structure. ^{1}H,^{15}N HSQC spectra of Sac7d and the V30I mutant showed only small chemical shift differences for the NH and amide nitrogen atoms for residues in the immediate vicinity of the cavity (Figure 3). There was also negligible change in the far UV CD spectrum (data not shown).

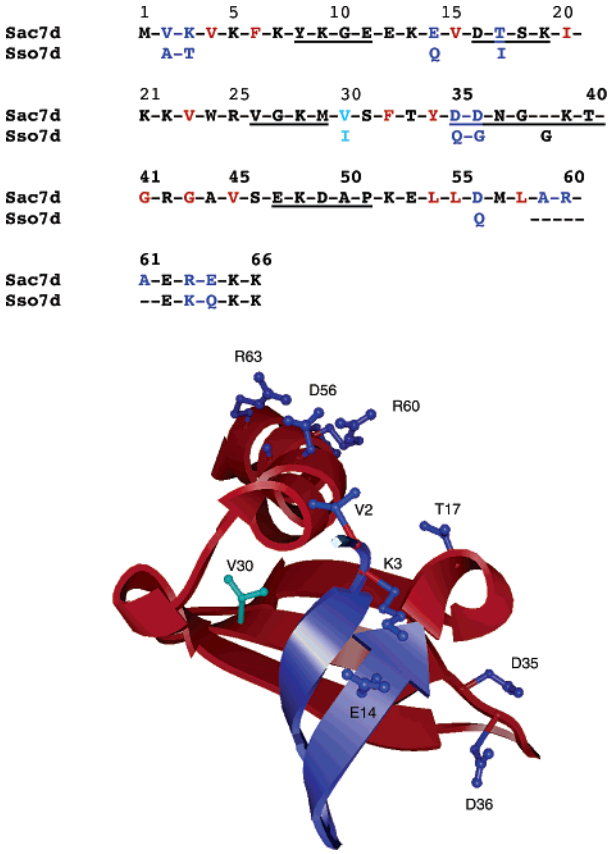

FIGURE 1: Locations of differences in the sequences of Sac7d (*50*, *88*) and Sso7d (*89*). Only those residues in Sso7d that differ from Sac7d are shown below the Sac7d sequence (in dark blue). Core residues are indicated in the sequence in red, except for V30 (I30 in Sso7d), which is colored light blue. The positions of the amino acid sequence differences are indicated by the side chains in the Sac7d NMR solution structure (1sap). The two-stranded β-ribbon is shown in blue only to assist viewing the structure. Numbering is for recombinant Sac7d with an initiating methionine. Sso7d contains an additional glycine following G38 in an exposed loop (D35-T40 in Sac7d) between the second and third strands of the β-sheet, and three residues are deleted in the C-terminal α-helix. Underlined sequences indicate turns and loop regions.

Sso7d is a homologue of Sac7d from the more thermophilic *Sulfolobus solfataricus*, which has an optimal growth temperature about 5−10° higher than *S. acidocaldarius* (Deutsche Sammlung von Mikroorganismen und Zelkulturen GmbH, http://www.dsmz.de). Sso7d differs from Sac7d with 10 conservative residue substitutions, a glycine insertion in an exposed loop, and three amino acid deletions leading to a shortening of the C-terminal helix (Figure 1). Of primary interest here is the substitution of isoleucine for valine at position 30, the only difference in the hydrophobic core residues of Sso7d and Sac7d (*64*, *65*).

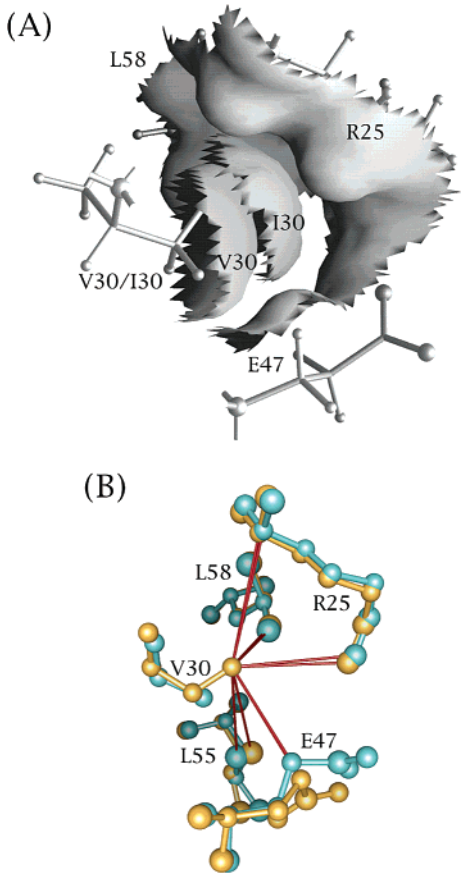

FIGURE 2: Structures of the hydrophobic core of Sac7d and Sso7d in the vicinity of residue 30. (A) Surfaces of atoms surrounding an internal cavity in Sac7d (1sap) are shown defined by V30, L58, E47, R25, A50, and L55 (surfaces for A50 and L55 are not shown for clarity). The effect of a V30I mutation is modeled by substitution of Ile without altering χ_1. (B) Positions of amino acid side chains around residue 30 in Sac7d and Sso7d. The X-ray crystal structures of Sac7d (blue, 1azp, 1.6 Å resolution) and Sso7d (yellow, 1bnz, 2.0 Å) were aligned using C atoms within 5 Å of the C_δ of I30 of Sso7d and the corresponding atoms in Sac7d. Red vectors indicate the following distances from a reference point defined by the isoleucine C_δ methyl position in Sso7d to selected atoms: R25 C_α: 4.4 Å (Sac7d) and 4.3 Å (Sso7d), R25 C_ζ: 4.0 Å (Sac7d) and 3.7 Å (Sso7d), E47 C_γ: 3.6 Å (Sac7d) and 4.2 Å (Sso7d), L55 $C_{\delta 2}$: 4.8 Å (Sac7d) and 4.9 Å (Sso7d), and L58 $C_{\delta 2}$: 3.4 Å (Sac7d) and 3.9 Å (Sso7d).

Comparison of the high-resolution crystal structures of Sac7d and Sso7d[3] (DNA complexes 1azp and 1bnz, respectively) indicates that the two proteins have nearly identical side chain positions in the vicinity of residue 30 (whether it is Val or Ile). This strongly supports the data above indicating that the Val → Ile substitution at residue 30 in Sac7d fills the adjacent cavity with only a slight perturbation (<0.5 Å) in the surrounding structure (Figure 2B). The same argument also indicates that the reverse mutation, I30V, in Sso7d should lead to cavity formation similar to that in Sac7d with contraction of the core by less than 0.5 Å.

[3] The NMR solution structures of Sac7d (1sap) and Sso7d (1sod) are of different resolutions and cannot be used to support a comparison of side chain positions. It has not been possible to obtain crystals of Sac7d and Sso7d in the absence of DNA. The NMR solution structure of Sac7d (1sap, free of DNA) and 1.6 Å crystal structures of Sac7d (1azp, complexed with DNA) show little difference in structure, with an RMSD for the C_α's from R25 to E58 of 1.05 Å (1.7 Å from K5−R60).

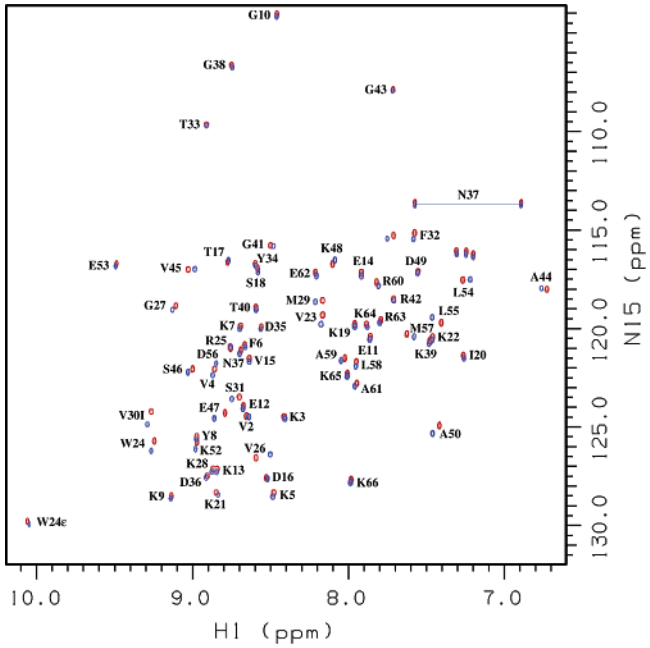

FIGURE 3: Overlay of ^1H,^{15}N HSQC spectra (800 MHz ^1H) of Sac7d (blue) and the V30I mutant (red) collected at pH 4 with 0.3 M KCl at 30 °C. Only minor differences are observed between the two spectra, with the largest changes originating from residues either nearby in the three-stranded β-sheet (W24 and A44) or lining the cavity filled by the substitution (A50, L55, E47).

We have made the I30V mutant of Sso7d and observed little change in the ^1H,^{15}N HSQC spectrum, indicating little change in structure (Figure S2, Supporting Information). Negligible change in the far UV CD spectrum was also observed (data not shown).

Differential scanning calorimetry indicated that thermal unfolding of Sac7d occurs reversibly with a T_m of 90.7 °C, and equal calorimetric and van't Hoff enthalpies of 58.5 kcal/mol at pH 7 in 0.3 M KCl (*47*) (DSC data are shown in Figure S1, Supporting Information). Sso7d unfolded reversibly by DSC with a T_m of 99 °C and an enthalpy of unfolding of 65.0 kcal/mol (in 0.3 M KCl, pH 7). The V30I substitution in Sac7d led to an increase in thermal stability with a T_m of 96.5 °C and a ΔH of 63 kcal/mol. A higher thermal stability of the V30I mutant was observed from pH 0 to 7 in 0.3 M KCl, with an average difference in T_m of approximately +6.5 °C (Figure 4). The I30V substitution in Sso7d led to a decrease in T_m to 95.1 °C (pH 7) with an unfolding enthalpy of 62.5 kcal/mol (Supporting Information). The Sso7d I30V substitution also led to a consistent decrease in T_m from pH 0 to 7, with an average difference of about −4.5 °C (Figure 4). Note that the steeper dependence of the T_m values of Sac7d and V30I on pH led to an intersection of the T_m vs pH curves for the V30I and I30V mutants at approximately pH 3.5 so that V30I had a higher thermal stability at pH 7 but a lower stability below pH 3 (see Discussion).

The pH-induced variation of the enthalpy of unfolding with T_m for all four proteins was linear within experimental error (Figure 5) giving apparent ΔC_P values (using the Kirchhoff relation (*66*)) for unfolding of Sac7d, V30I, I30V, and Sso7d of 496 (±21), 508 (±26), 467 (±31), and 545 (±29) cal/deg·mol, respectively (errors in parentheses are standard deviations from linear regression of the data). As shown below, these apparent ΔC_P values reflect the unfolding of

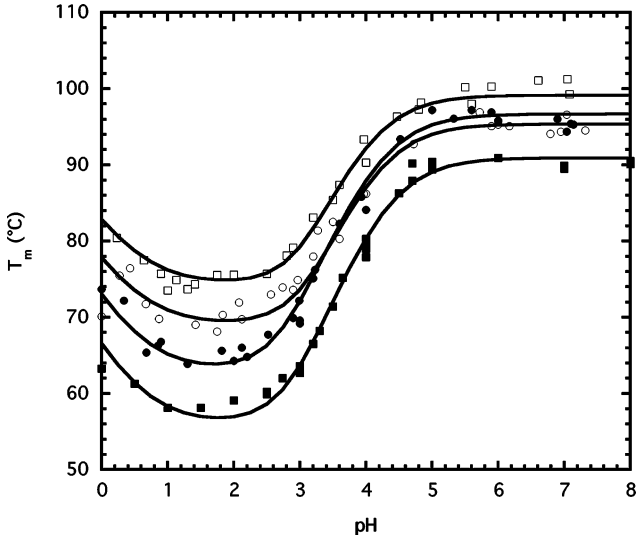

FIGURE 4: pH dependence of the T_m from DSC of Sac7d (■), V30I (●), Sso7d (□), and I30V (○) at 0.3 M KCl. The difference between the Sac7d and V30I curves (and also the Sso7d and I30V) curves is nearly constant from pH 0 to 8, indicating a vertical offset of the free energy surfaces along the pH dimensions, i.e., there is little effect of pH and anion concentration on the difference in stability created by the mutations.

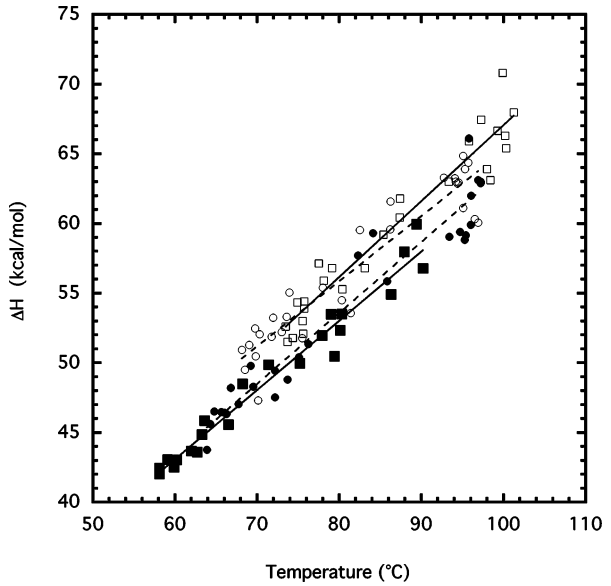

FIGURE 5: Kirchhoff plots (ΔH vs T_m) for Sac7d (■), V30I (●), Sso7d (□), and I30V (○) in 0.3 M KCl. Linear fits of the native protein data are indicated by the solid lines, and that of the mutant proteins by dashed lines. The data were taken from the same DSC experiments used for Figure 4, i.e., the stability of each protein was varied by changing the pH. The increased anion binding at low pH contributes to the observed heats of unfolding such that the slopes, $\partial\Delta H/\partial T_m$, do not reflect the ΔC_P of the intrinsic unfolding reaction N → U.

the protein as well as changes in protonation and chloride binding associated with acid-induced folding at lower pH. The enthalpy of unfolding V30I was essentially identical to that of Sac7d between 60 and 100 °C, and a linear fit of the combined Sac7d and V30I data (50 data points) gave an apparent ΔC_P of 511 (±16) cal/deg·mol. Similarly, the enthalpy of unfolding Sso7d was essentially identical with that of Sso7d I30V over the measured temperature range, and a linear fit of the combined data (56 data points) gave an apparent ΔC_P of 507 (±21) cal/deg·mol. The displacement

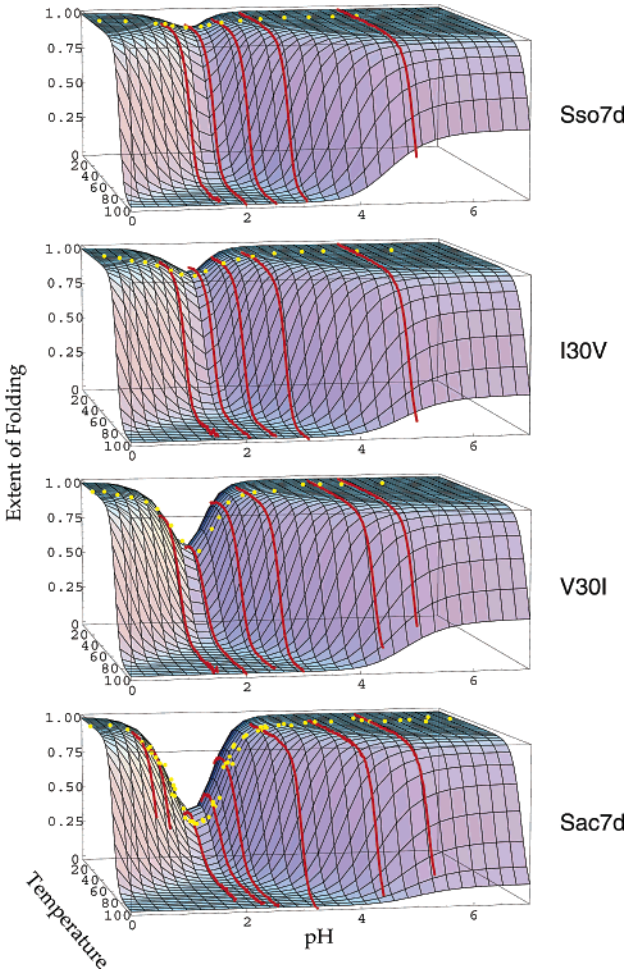

FIGURE 6: Dependence of unfolding of Sac7d, V30I, I30V, and Sso7d as a function of pH and temperature followed by CD at 205 nm. Solid curves show thermal unfolding at various pH values, and solid yellow circles show the pH dependence of folding at 20 °C. The extent of folding was obtained from the observed CD at 205 nm, $\Delta\epsilon_{obs}^{205}$, according to $(\Delta\epsilon_{obs}^{205} - \Delta\epsilon_U^{205})/(\Delta\epsilon_N^{205} - \Delta\epsilon_U^{205})$, where $\Delta\epsilon_N^{205}$ is the maximal CD observed at 205 nm at 20 °C and pH 7, and $\Delta\epsilon_U^{205}$ is the CD of the unfolded state at 20 °C obtained by extrapolating the high-temperature baseline at pH 2 to 20 °C (*55*). The surfaces are the results of fitting all of the data in Figures 4, 5, and here by a global linkage analysis of each protein and the resulting parameters are given in Table 1.

of the Sac7d and Sso7d curves indicates a constant difference of 2.7 kcal/mol between 60 and 100 °C.

Sac7d unfolds with decreasing pH in the absence of salt, reaching maximal unfolding (about 75%) at pH 2 (*47*, *55*). The pH dependence of unfolding was most conveniently followed by CD, and the results obtained for V30I, I30V, and Sso7d are compared to those for Sac7d in Figure 6 (solid yellow circles). The increased charge density on these highly basic proteins under acidic conditions leads to chloride binding and stabilization of a folded protein with acid-induced refolding becoming obvious below pH 2. The amount of protein remaining folded at pH 2 indicated a progressive increase in stability in going from Sac7d to V30I to I30V and finally Sso7d. The negligible unfolding of Sso7d at pH 2 has made it difficult to observe the contributions of linkage of protonation and anion binding to folding in previous studies of this protein (*49*, *67*). Note that the order of stability is consistent with that implied by the T_m's at pH

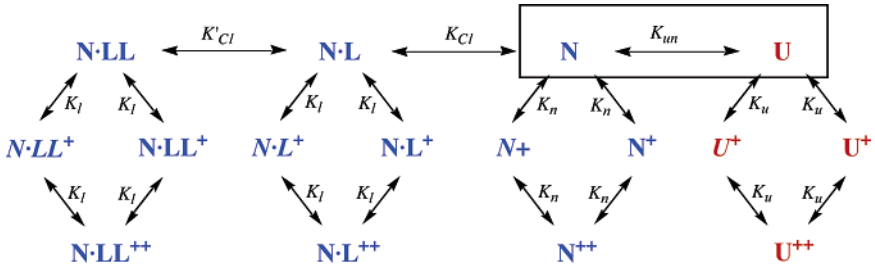

FIGURE 7: The minimal linkage model used to fit the CD and DSC stability data for Sac7d, Sso7d, and the residue 30 mutants. Equilibrium constants for the reactions indicated explicitly with double arrows are defined in the model. Equilibrium constants for all other reactions are defined by products of the defined constants. The intrinsic N−U unfolding reaction (described by K_{un} and outlined by the solid box) predominates at pH 7. With decreasing pH, carboxyl groups in the native folded (N), and unfolded (U) species become protonated and chloride binding is promoted. Unfolding at lower pH is characterized by the conversion of an ensemble of N species (blue) to an ensemble of U species (red). The model includes the binding of two chloride ions and two carboxyl protonations linked to protein folding. Other protonation and chloride binding sites certainly exist, but at least two are linked to folding. Chloride binding to the first and second sites is described by the binding constants K_{Cl} and K'_{Cl}, respectively, leading to N·L and N·LL species. Protonation of the first carboxyl in U, N, N·L, and N·LL is indicated with a superscript "+" (to indicate an increase in charge by +1, the total charge on the protein depends on the pH), and protonation of both sites 1 and 2 by "++". In the minimal model used here the pK's of the two linked carboxyls are assumed to be identical but vary with folding and chloride binding (viz. pK_u, pK_n, and pK_1). Differences in the order of protonation are indicated by normal and italic symbols, e.g., U^+ and U^+.

Table 1: Thermodynamic Parameters Characterizing the Temperature, pH and Salt Dependence of the Stability of Sac7d, V30I, Sso7d, and I30V[a]

parameter	Sac7d	V30I	Sso7d	I30V
		Intrinsic Unfolding Reaction		
T_m (°C)	90.7 (±0.1)	96.5 (±0.1)	99.0 (±0.1)	95.1 (±0.1)
$\Delta H(T_m)$ (kcal/mol)	58.5 (±1.0)	63.0 (±1.7)	65.0 (±1.5)	62.5 (±1.75)
ΔC_P (cal/deg·mol)	711 (±19)	755 (±19)	751 (±19)	710 (±19)
		Chloride Binding Constants, and Associated Heats and Heat Capacity Changes		
pK_{Cl} (0.0 M KCl)	−0.14 (±0.06)	−0.21 (±0.07)	−0.10 (±0.1)	−0.23 (±0.05)
pK'_{Cl} (0.0 M KCl)	1.84 (±.07)	2.51 (±0.09)	−5.1 (−∞ → 1.2)	−10.3 (−∞ → 0.2)
pK_{Cl} (0.3 M KCl)	−0.14 (±0.5)	0.23 (±0.35)	0.06 (±0.3)	−0.1 (±0.4)
ΔH (cal/mol)	−676 (±1315)	−270 (±1684)	−904 (±1160)	−258 (±933)
ΔC_P (cal/deg·mol)	−101 (±122)	−56 (±91)	−101 (±77)	−134 (±85)
		pK's of Linked Carboxyls in the Unfolded Protein		
pK_u (0.0 M KCl)	4.67 (±0.15)	4.53 (±0.02)	4.35 (±0.02)	4.50 (±0.02)
pK_u (0.3 M KCl)	4.45 (±0.19)	4.39 (±0.18)	4.08 (±0.14)	4.11 (±0.18)
		pK's of Linked Carboxyls in the Folded Protein		
pK_n	0.01 (−∞ → 1.2)	0.1 (−∞ → 1.2)	0.09 (−∞ → 1.5)	0.09 (−∞ → 1.5)
		pK's of Linked Carboxyls in the Folded Protein with Bound Chloride Ions		
pK_1 (0.0 M KCl)	2.98 (±0.03)	2.53 (±0.04)	3.14 (±0.06)	3.26 (±0.05)
pK_1 (0.3 M KCl)	3.15 (±0.6)	3.31 (±0.25)	3.35 (±0.28)	3.42 (±0.44)

[a] The T_m and $\Delta H(T_m)$ values for the intrinsic unfolding reaction were fixed during a global fit to the experimental values measured from DSC at pH 7 (above the pH range where linkage of carboxyl and chloride binding contribute). The ΔH and ΔC_P values for acid protonation were fixed to the published values for acetate (*55*). Chloride binding constants are reported as pK_{Cl}, i.e., the log of the binding constant. All protonation and chloride binding pK's, ΔH and ΔC_P values are defined at 25 °C. Errors in parentheses (except for T_m, $\Delta H(T_m)$, and ΔC_P) are the precision limits determined by the variation required to increase the reduced χ^2 by 1.0 (*58*). The error in T_m is the estimated experimental error from repeated DSC measurements. The error for $\Delta H(T_m)$ was determined by the standard deviation of the residuals from a linear fit of $\Delta H(T_m)$ vs T_m (data in Figure 5). The errors in ΔC_P for Sac7d, V30I, Sso7d, and I30V were determined by the variation of the parameter required to increase the reduced χ^2 by 1.0 (±6, ±4, ±19, and ±12, respectively). As discussed in the text, the largest error of the four (±19) is used for all four ΔC_P values here.

2 in Figure 4, and not with the T_m's at pH 7. The significance of this will be discussed below.

CD was used to follow thermally induced protein unfolding at various values of pH in the absence of salt (red curves, Figure 6). The results are consistent with the variation of folding with pH at 20 °C (yellow solid circles, Figure 6), and confirm that V30I has a higher T_m at high pH, yet appears to have a lower stability at pH 2. The presence of a saddle in the vicinity of pH 2 is observed for all four proteins, and even though the depth of the saddle at pH 2 is small for Sso7d, the decrease in T_m in this pH region indicates that this protein also has a lower stability at pH 2. Its stability (i.e., ΔG) is high enough to make the change in folding equilibrium nearly imperceptible except at elevated temperatures (e.g., above 30 °C).

We have previously shown that the pH, salt, and temperature dependence of the stability of Sac7d can be fit with a model that includes the linkage of carboxyl ionization, chloride binding, and protein folding (*55*). As described in Materials and Methods, the *minimal model* capable of fitting the Sac7d data required that folding be linked to the protonation of two carboxyls and the binding of two chloride ions (Figure 7). Fits of the CD and DSC data for Sac7d, Sac7d V30I, Sso7d, and Sso7d I30V are presented in Figures 4 and 6, and the fitted parameters are provided in Table 1. Inspection of the parameters for Sac7d and V30I shows few significant changes (*within the error limits*) in the parameters characterizing chloride binding and carboxyl ionization reactions. A slight change in electrostatic interactions is indicated by a small change in one of the apparent chloride

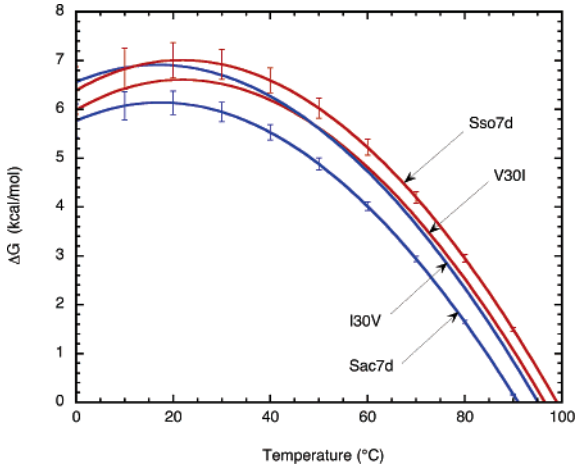

FIGURE 8: Fitted protein stability curves for Sac7d, V30I, I30V, and Sso7d at pH 7. The curves corresponding to proteins with valine at residue 30 are shown in blue, and those with isoleucine are shown in red. The temperature dependence of the errors are shown with error bars for Sac7d and Sso7d, calculated using eq 6. Errors for V30I and I30V mutants are of similar magnitude and are not shown for clarity.

binding constants and the apparent p*K* of the carboxyls in the folded protein with bound chloride. For both Sso7d and I30V, the significantly negative values for the second pK_{Cl} indicate that a second chloride binding site at low salt was not necessary to fit the data.

Most interesting is the small, but significant, increase in ΔC_P for the intrinsic unfolding reaction as a result of the Val → Ile substitution (T_m and ΔH at the T_m were held fixed to the values determined by DSC at pH 7). *ΔC_P was consistently one of the best defined parameters in the global fit*. Similarly, ΔC_P showed a significant decrease resulting from the I30V core substitution in Sso7d. ΔC_P values for the two proteins with valine at position 30, i.e., Sac7d and Sso7d I30V, were essentially identical (viz. 711 cal/deg·mol and 710 cal/deg·mol, respectively; estimated error ±19 cal/deg·mol, see Error Analysis in Methods). Values for the two proteins with isoleucine at position 30, i.e., Sso7d and Sac7d V30I, were also essentially identical (viz. 751 and 755 cal/deg·mol, respectively; estimated error ±19 cal/deg·mol).

A global analysis provides an accurate and precise fitting of the overall protein folding free energy (ΔG_{unf}) surface as a function of temperature, pH, and salt. ΔG_{unf} reflects the intrinsic unfolding energy as well as the effects of carboxyl ionization and chloride binding, i.e., it is the global free energy commonly reported for protein folding. The fitted free energy surfaces for the four proteins as a function of temperature, pH, and salt concentration differ due to both vertical and lateral shifts. The surfaces are shifted to higher energy progressively from Sac7d, then Sac7d V30I, Sso7d I30V, and finally Sso7d (data not shown). Cross-sections through the surfaces at 20 °C as a function of pH at both high and low salt clearly show a nearly constant displacement from pH 0 to 8 (Figure S3, Supporting Information), *indicating little change in carboxyl protonation or chloride binding energetics as a result of the core mutations*. Comparison of the protein stability curves (ΔG as a function of temperature) shows a lateral displacement as well as vertical. These curves fall into two groups, one centered near 17 °C (blue curves in Figure 8) and the other near 21 °C (red curves). The lower temperature group contains valine at position 30, while the upper temperature group contains isoleucine at this position. The two proteins with Ile at position 30 have a higher temperature of maximal stability, greater T_m's, and also display greater curvature in the stability curve. The average intrinsic ΔC_P of unfolding for the proteins with valine at position 30 is 710 (±19) cal/deg·mol, while that for the isoleucine is 753 (±19) cal/deg·mol.

Finally, it is appropriate to stress the necessity of the linkage model in fitting the free energy surface for Sac7d and Sso7d. The difference in the unfolding free energies due to the substitution of Ile for Val at position 30 would not be apparent in a conventional analysis of DSC data. Within experimental error, the variation of ΔH with T_m shown in Figure 5 provides virtually identical apparent ΔC_P's for all four proteins, viz. 509 (±13) cal/deg·mol, and no change in ΔH due to the substitutions. Using the T_m and observed ΔH values from DSC with this apparent ΔC_P would lead to protein stability curves that are simply displaced vertically with identical curvature (and T_{max} values) (and an inaccurate representation of the differences in stability at lower temperature). The stability curves for I30V and V30I predicted using a ΔC_P of 509 cal/deg·mol do not intersect as required by the dependence of T_m on pH data (Figure 4). The predicted stability curves would not be in agreement with the extent of unfolding indicated by CD at lower temperature and pH (solid yellow circles in Figure 6). In addition, the protein stability curves would show a maximum in stability well below 0 °C, while the thermal unfolding followed by CD at pH 2 shows a maximum in stability near 20 °C. A similar T_{max} was observed in the temperature dependence of the ΔG of unfolding determined by chemical denaturation (*47*). The observation of a higher temperature of maximal stability than expected using the apparent ΔC_P value cannot be attributed to a temperature-dependent ΔC_p since there is no indication of nonlinearity in the Kirchhoff plots (Figure 5). A 50% increase in ΔC_P from 500 to 750 cal/deg·mol with decreasing temperature would be apparent in these plots.

DISCUSSION

The importance of packing and hydrophobicity in the thermophile proteins Sac7d and Sso7d has been investigated using V/I core substitutions. The small size of these proteins (and corresponding smaller thermodynamic parameters associated with folding) makes it possible, in principle, to measure small differences in not only the ΔG of unfolding, but also changes in ΔG, ΔS, and ΔC_P resulting from single-site core mutations. The changes observed here for ΔC_P (and also ΔH, ΔS, and ΔG as discussed below) are at the limit of the reliability of such measurements even with extensive data, and care has been taken to describe the errors in the measurements. Most importantly, the excellent agreement between the thermodynamic changes observed for the V30I substitution in Sac7d and those observed for the reverse mutation in the homologous Sso7d (Figure 9) with independent data sets and different stabilities supports the reliability of the measurements and the level of precision indicated by the error analysis.

We concentrate here on the temperature dependence of the energetics of the intrinsic unfolding reaction, i.e., the unfolding reaction after deconvolution of the thermodynamic

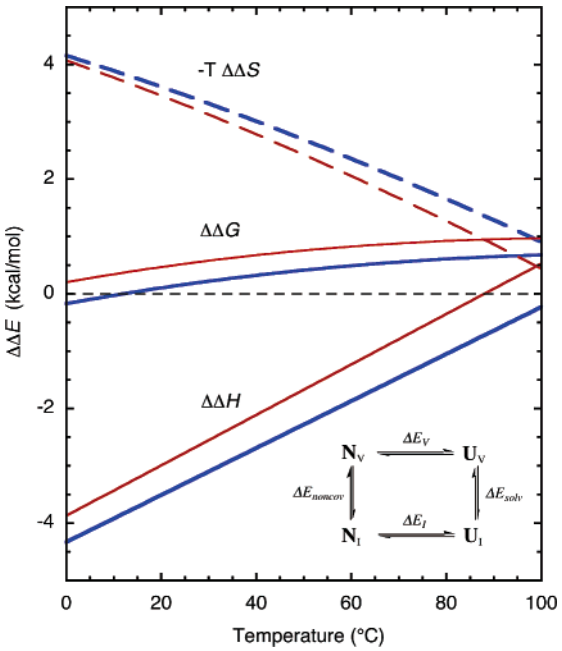

FIGURE 9: The temperature dependence of $\Delta\Delta G$, $\Delta\Delta H$, and $T\Delta\Delta S$ (referred to collectively as $\Delta\Delta E$) as a result of changing the hydrophobicity of residue 30 in Sac7d and Sso7d. Red curves correspond to changes associated with the cavity-filling Sac7d → V30I substitution, and blue curves correspond to the cavity-filling substitution I30V → Sso7d. ΔG, ΔH, and ΔS values were calculated using eqs 1−3 (Materials and Methods) with the thermodynamic parameters for the intrinsic unfolding reaction in Table 1. The thermodynamic cycle in the inset shows the reactions used for calculating the differences due to cavity filling where $N_V \rightarrow U_V$ refers to the unfolding of the species with V at position 30, and $N_I \rightarrow U_I$ refers to that with I. $\Delta\Delta E$ values were calculated for small to large reactions. For I30V → Sso7d, $\Delta\Delta E = \Delta E_I$(Sso7d) − ΔE_V(I30V); and for Sac7d → V30I, $\Delta\Delta E = \Delta E_I$(V30I) − ΔE_V(Sac7d), where $\Delta E = E_U - E_N$. Errors in $\Delta\Delta E$ values, calculated as described in Materials and Methods, are as follows: for Sac7d → V30I at 50 °C, $\sigma_{\Delta\Delta G} = 0.25$ kcal/mol, $\sigma_{\Delta\Delta H} = 2.3$ kcal/mol, $\sigma_{T\Delta\Delta S} = 2.0$ kcal/deg·mol; for I30V → Sso7d at 50 °C, $\sigma_{\Delta\Delta G} = 0.3$ kcal/mol, $\sigma_{\Delta\Delta H} = 2.6$ kcal/mol, $\sigma_{T\Delta\Delta S} = 2.3$ kcal/deg·mol.

contributions of protonation and anion binding. The characterization of the dependence of protein stability on pH and salt concentration indicates that the core substitutions at residue 30 do not appear to lead to significant modifications of surface electrostatic interactions, and changes in stability can be attributed to modifications of the core packing and/or hydrophobicity. This is not always the case, and in some proteins substitutions of core aliphatic residues have been shown to induce changes in surface electrostatics (*68*, *69*).

The effect of the core mutations in Sac7d and Sso7d is consistent with changes in hydrophobicity with no need to invoke changes in van der Waals (packing) interactions. The results are conveniently discussed in terms of changes in the ΔG, ΔH, and $T\Delta S$ of the intrinsic unfolding reaction (i.e., $\Delta\Delta G$, $\Delta\Delta H$, and $T\Delta\Delta S$; Figure 9) from the perspective of small to large substitutions, i.e., for Sac7d → V30I: $\Delta\Delta E = \Delta E_I$(V30I) − ΔE_V(Sac7d), and for Sso7d I30V → Sso7d: $\Delta\Delta E = \Delta E_I$(Sso7d) − ΔE_V(I30V) (where $\Delta E = E_U - E_N$ refers to changes in G, H, and S for the intrinsic N → U unfolding reaction). We assume negligible differences in residual structure in the *unfolded* chains, and all noncovalent interactions are attributed to hydration differences in the unfolded state along with differences in van der Waals contacts in the folded protein and reduced entropy of the restricted side chain in the core. Consideration of the thermodynamic cycle in the inset to Figure 9 (see ref 42) demonstrates that $\Delta\Delta E$ is equal to $\Delta E_{solv} - \Delta E_{noncov}$ (where ΔE_{solv} is the solvation energy of the larger side chain minus that for the smaller in the unfolded protein, and ΔE_{noncov} is the difference in noncovalent interaction energy of the larger side chain in the folded protein minus that for the smaller). For mutations involving Val/Ile substitutions, ΔE_{solv} represents differences in hydration or the hydrophobic contribution, and ΔE_{noncov} represents differences in the van der Waals interactions (packing) and side chain entropies (and conformational changes that structural data indicate to be small). Both cavity-filling transitions are stabilizing in terms of ΔG, i.e., the free energy of unfolding the Ile variant is greater than that with Val over the available temperature range (and $\Delta\Delta G > 0$) (Table 2). The free energy gained from small-to-large substitutions becomes increasingly favorable with increasing temperature and reaches a maximum around 116 °C (Figure 9). At 50 °C the increase in stability due to the V30I substitution was 0.7 (±0.2) kcal/mol for Sac7d, and the decrease in stability resulting from the I30V substitution in Sso7d was 0.4 (±0.3) kcal/mol (average change of 0.6 kcal/mol per methylene). These values are about half those commonly reported for the contribution of a methylene group to the stability of a protein (*32*, *40*, *46*, *70*), but are in good agreement with the difference in transfer free energy measurements for Ile and Val from octanol to water (*71*, *72*).

van der Waals interactions and packing do not appear to play a major role in determining the advantage of Ile over Val in these proteins. The enthalpy of unfolding Sac7d and Sso7d with Ile at position 30 was less than that with Val in this position, so that $\Delta\Delta H$ is negative (within the defined error limits) over most of the temperature range, i.e., small-to-large substitutions are enthalpically unfavorable (Figure 9). Enhanced van der Waals interactions would be enthalpically favorable. In addition, the temperature dependence of $\Delta\Delta H$ is inconsistent with van der Waals interactions, which are largely temperature independent (*30*). $T\Delta\Delta S$ values are also negative over most of the temperature range making cavity-filling entropically favorable. Increased van der Waals interactions due to optimized packing would be expected to be associated with positive $\Delta\Delta H$ and $\Delta\Delta S$ values, and be enthalpically dominated (*30*, *46*).

Substitution of Ile for Val should destabilize the folded state by about 0.5 kcal/mol due to the greater entropy of the Ile side chain in the unfolded state (*73*). The temperature dependence of this effect is negligible over the temperature range studied here (*30*). In contrast, van der Waals contacts contributed by the additional methylene in Ile can be expected to stabilize the folded state due to a decrease in enthalpy on the order of 0.5 kcal/mol (30 cal/mol·Å^2 * 23 Å^2, with no change in entropy due to the van der Waals interaction) (*30*). The temperature dependence of van der Waals interactions is also negligible over the range studied here. Therefore, to a first approximation, increased van der Waals interactions for V/I substitutions are balanced by the penalty of restricting the Ile side chain upon folding.

The above considerations indicate that $\Delta\Delta E$ for cavity filling in Sac7d (particularly $\Delta\Delta G$) should be largely determined by $\Delta E_{sol} = E_U$(Ile) − E_U(Val), i.e., the energy of hydration of a methylene group. Indeed, the signs and

Table 2: Changes in the Thermodynamics of Unfolding Sac7d and Sso7d as a Result of Cavity Filling, Comparison to Differences in Hydration of Val and Ile, and Selected Results on Other Proteins[a]

small to large substitution	$\Delta\Delta G$ (kcal/mol)	$\Delta\Delta H$ (kcal/mol)	$-T\,\Delta\Delta S$ (kcal/mol)	$\Delta\Delta C_P$ (cal/deg·mol)
Sac7d → Sac7d V30I	0.7	−1.7	2.4	44
Sso7d I30V → Sso7d	0.4	−2.3	2.7	41
V → I[b] (hydration)	0.3	−0.4	0.7	12
leucine zipper $(A12)_2$ → A_2 (Ala → Leu) (*83*)	2.9	1.4	1.3	52
RNase S I13V → RNase S (*42*)	0.2	1.9	−1.7	40
ubiquitin L67A → ubiquitin (*46*)	2.8	6.2	3.4	−24
barnase I96V → barnase (*40*)	0.9	1.1	−0.2	*c*
CI2 I39V → CI2 (*38*)	1.2	1.8	−0.6	*c*
T4 lysozyme I27A → T4 lysozyme (*37*)	2.7	18.8	−16.1	*c*
T4 lysozyme → T4 lysozyme AMH (*44*)	0.5	3.6	−3.0	*c*
c-Myb → c-Myb V103I (*35*)	0.7	0.2	0.5	*c*

[a] All thermodynamic values are reported at 50 °C, except for the RNase values which are at 25 °C. All $\Delta\Delta E$ differences are reported for cavity-filling substitutions by subtracting the ΔE for unfolding the protein containing the smaller residue from that with the larger, e.g., $\Delta\Delta E = \Delta E_{Ile} - \Delta E_{Val}$ where $\Delta E = E_U - E_N$. Thermodynamic parameters for barnase, CI2 (chymotrypsin inhibitor 2), and T4 lysozyme were calculated using the Gibbs−Helmholtz equation with the following values from the literature: barnase (*40*): $\Delta C_P = 1.2$ kcal/deg·mol, $T_m = 53.9$ °C, $\Delta H(T_m) = 125$ kcal/mol; barnase I96V (*40*): $\Delta C_P = 1.2$ kcal/deg·mol, $T_m = 51.5$ °C, $\Delta H(T_m) = 121$ kcal/mol; CI2 (*38*): $\Delta C_P = 720$ cal/deg·mol, $T_m = 73.8$ °C, $\Delta H(T_m) = 67$ kcal/mol, CI2 I39V (*38*): $\Delta C_P = 720$ cal/degmol, $T_m = 67.3$ °C, $\Delta H(T_m) = 61.5$ kcal/mol; T4 lysozyme (*37*): $\Delta C_P = 1800$ cal/deg·mol, $T_m = 51.7$ °C, $\Delta H(T_m) = 113$ kcal/mol; T4 lysozyme I27A: $\Delta C_P = 1800$ cal/deg·mol, $T_m = 41.6$ °C, $\Delta H(T_m) = 76$ kcal/mol, T4 lysozyme (*44*): $\Delta C_P = 2500$ cal/deg·mol, $T_m = 43.5$ °C, $\Delta H(T_m) = 96$ kcal/mol, T4 lysozyme L133−2-amino-4-methylhexanoic acid: $\Delta C_P = 2500$ cal/deg·mol, $T_m = 45.4$ °C, $\Delta H(T_m) = 103$ kcal/mol; c-Myb: $\Delta C_P = 322$ cal/deg·mol, $T_m = 39.6$ °C, $\Delta H(T_m) = 31.8$ kcal/mol; c-Myb V103I: $\Delta C_P = 322$ cal/deg·mol, $T_m = 46.6$ °C, $\Delta H(T_m) = 34.3$ kcal/mol. Engineered leucine zipper A_2 and $(A12)_2$ values were taken from Figures 4 and 6 of Durr and Jelesarov (*83*) and divided by 2 to adjust for the two mutations in the homodimer. RNase S I13V $\Delta\Delta E$ values were taken directly from Ratnaparkhi and Varadarajan (*42*). Values for ubiquitin were taken directly from Loladze et al. (*46*). $\Delta\Delta C_P$ for ubiquitin was too small to measure accurately. Errors in $\Delta\Delta G$, $\Delta\Delta H$, and $T\Delta\Delta S$ for Sac7d and Sso7d are given in Figure 9. Errors in the literature values for $\Delta\Delta G$ are typically on the order of 0.1 to 0.3 kcal/mol. Errors in $\Delta\Delta H$ and $\Delta\Delta S$ from the literature are commonly not reported, and are estimated here to be of the same order of magnitude as the values of $\Delta\Delta H$ and $\Delta\Delta S$ based on the estimated error in individual measurements of ΔH by calorimetry or van't Hoff methods. The error in the $\Delta\Delta C_P$ values for Sac7d and Sso7d mutations are estimated to be 27 cal/deg·mol using standard propagation of error formulas (*58*). The reported errors in the literature values for $\Delta\Delta C_P$ are 40 cal/deg·mol for Rnase S (*42*) and 32 cal/deg·mol for the $(A12)_2$ dimer (*83*). [b] Differences in the thermodynamics of hydration of Val and Ile were calculated at 50°C using values for ΔH, $T\Delta S$, ΔG, and ΔC_P from Figure 9 of Makhatadze and Privalov (*30*) and a difference in surface area of 23 Å^2 (*77*). [c] Differences in ΔC_P as a result of the mutation in barnase, CI2, c-Myb, and T4 lysozyme were assumed to be zero in the original work.

temperature dependences of $\Delta\Delta G$, $\Delta\Delta H$, and $-T\Delta\Delta S$ are similar to those of ΔG, ΔH, and $-T\Delta S$ of hydration of aliphatic molecules (*27*, *30*, *74*−*76*). Compare, for example, Figure 9 to Figure 9A in a review by Makhatadze and Privalov (*30*). Both $\Delta\Delta G$ for cavity filling and ΔG of hydration for a methylene group are positive and on the order of 0.5 kcal/mol at 50 °C. ΔG of hydration of nonpolar surface area increases with temperature and reaches a maximum around 125 °C. Both $\Delta\Delta H$ for cavity filling and ΔH of aliphatic solvation are negative (and of comparable magnitude given the error in $\Delta\Delta H$) at 50 °C. Similarly, $-T\Delta\Delta S$ for cavity filling and $-T\Delta S$ of aliphatic solvation are positive and of comparable magnitude (within the defined error limits). The entropically dominated benefit of cavity filling is consistent with the dominant role of entropy in favoring hydration of Val over Ile. In addition, $\Delta\Delta H$ and $T\Delta\Delta S$, as well as ΔH and ΔS of aliphatic solvation, are strongly dependent on temperature with a positive ΔC_P, another indicator of hydrophobic interactions. T_H, the temperature at which $\Delta\Delta H$ passes through zero, is about 97 °C (88 °C for Sac7d−V30I, and 106 °C for I30V−Sso7d), and T_S, the temperature at which $-T\Delta\Delta S$ passes through zero, is about 116 °C (110 °C for Sac7d−V30I and 123 °C for I30V−Sso7d). In comparison, T_H for the aliphatic hydration enthalpy is around 81 °C, while the corresponding T_S for the hydration entropy is around 125 °C.

The difference in ΔC_P measured here for the Val → Ile substitution is somewhat greater than the ΔC_P expected from differences in the hydration of the amino acids. Makhatadze and Privalov (*30*) report a ΔC_P for nonpolar aliphatics of about 0.5 cal/mol·deg·Å^2 based on thermodynamics of transfer to water for more than a hundred organic molecules. A Val-to-Ile substitution results in a change in nonpolar surface area of 23 Å^2 (*77*), which translates into an increase in ΔC_P of about 12 cal/deg·mol. Similar values for ΔC_P are calculated (ranging from 6.4 to 12 cal/deg·mol) using the empirical equations of Murphy and Freire (*78*), Makhatadze and Privalov (*30*), Spolar et al. (*79*), and Myers et al. (*80*). Considering the estimated error in the $\Delta\Delta C_P$ values (i.e., 27 cal/deg·mol), the difference between the experimental $\Delta\Delta C_P$ values determined here and those predicted from model compound data (*30*, *78*, *79*) as well as protein data (*80*) is not great. It may reflect the limited sampling of two mutations. Alternatively, the larger than expected changes in ΔC_P may reflect higher vibrational contributions to the heat capacity of the folded state of the proteins containing cavities, and therefore a smaller ΔC_P upon unfolding (*68*, *81*). Although there is a good correlation between the ΔC_P for protein unfolding and the change in accessible surface area (*79*), the range of observed ΔC_P values for a given ΔASA is quite large (approaching 1000 cal/deg·mol (*63*, *80*)). It would appear that there are significant contributions to the ΔC_P of protein unfolding and changes in solvent exposure of hydrophobic groups in addition to changes in solvent-accessible surface area.

We have shown that a large part of the increased stability of Sso7d relative to Sac7d is the increased hydrophobicity of the protein core due to a Val-to-Ile substitution of residue 30. While there have been a number of studies of the effects of cavity creation and filling in proteins, few have involved

precise measurements of ΔC_P and the temperature dependence of stability. Most notably, none have been consistent with a change in hydrophobicity (*42*). Representative results are presented in Table 2, and a comparison to the Sac7d and Sso7d results follows.

Core mutations in barnase and CI2 have been characterized using DSC or thermal unfolding followed with spectroscopic probes, assuming that cavity creation had no effect on the ΔC_P of unfolding (*38*, *40*). Results indicated that cavity creation was destabilizing because of a decreased enthalpy change, i.e., $\Delta\Delta H$ for cavity filling was positive (Table 2). The stability of a large number of T4 lysozyme mutants have been determined using thermal denaturation followed spectroscopically and assuming no change in ΔC_P (*37*, *82*). The magnitude of $\Delta\Delta H$ associated with most of the single amino acid substitutions in T4 lysozyme was extraordinarily large, indicating significant structural rearrangements. Similarly, a thorough study of *cavity creation* in the four α-helical bundle ROP (*68*) showed an unusually large change in ΔC_P, most likely due to significant changes in structure.

Changes in ΔC_P associated with *cavity creation* in an engineered leucine zipper A_2 have been measured in an elegant study by Durr and Jelesarov (*83*). The temperature dependence of the thermodynamic effect of cavity creation showed a decrease in ΔC_P of 52 cal/deg·mol per methylene group removed, in good agreement with that determined here. We note that the leucine zipper undergoes acid-induced folding, but the contribution of anion binding at low pH to the measured thermodynamic parameters was not determined. Neglect of anion binding may explain the positive $\Delta\Delta H$ for cavity filling observed for the $(A12)_2$ dimer (Table 2), or this may be due to extensive disruption of van der Waals packing interactions. Since van der Waals interactions are thought to be largely independent of temperature over the range studied here, the ΔC_P can be largely attributed to the hydrophobic effect.

Varadarajan and co-workers (*42*) used ITC to study the energetics of packing and cavity formation in RNase S. The method permits a direct measure of ΔC_P by varying temperature rather than pH, and the measured value of 40 cal/deg·mol for a Val-to-Ile substitution is in excellent agreement with the results reported here. The positive value for $\Delta\Delta H$ is similar to that observed for the engineered leucine zipper and may indicate disruption of van der Waals interactions beyond the cavity creation site.

Cavity-creating mutations in ubiquitin (*46*) led to a decrease in stability due to a decrease in enthalpy (on the order of 10% of the total enthalpy of unfolding) which was attributed to loss of van der Waals interactions (packing). The structure of ubiquitin has been argued to be optimized for stability (*46*, *84*), and thus core substitutions may be more detrimental than in Sac7d. In an earlier report (*45*), it was shown that the change in ΔC_P of unfolding due to cavity-creating mutations in ubiquitin could be either positive or negative (L67A $\Delta\Delta C_P = -24$ cal/deg·mol, V17A $\Delta\Delta C_P = +48$ cal/deg·mol), but the change was comparable to the estimated error limits of ±50 cal/deg·mol.

It is intriguing to consider why the stabilizing V30I substitution occurs naturally in Sso7d and not in Sac7d. *Sulfolobus solfataricus* grows optimally near 80 °C, with a maximal growth temperature of about 90°C. In contrast, *Sulfolobus acidocaldarius* grows optimally near 75 °C, with a maximal growth temperature between 80 and 85 °C. Sac7d is only marginally stable at the in vivo growth temperature where about 10% of the protein molecules would be unfolded. However, the protein is stabilized by binding to DNA. In vivo there may be no advantage to increasing the stability of the protein. It should be noted that the V30I substitution occurs on the opposite face of the β-sheet involved with DNA binding, near the intercalating V26 and M29 residues which create a 60 to 70° kink in DNA (*85*). It remains to be seen if the V30I substitution affects the flexibility of the DNA binding site.

We comment briefly here on the relationship between these results and previous work on Sac7d and Sso7d. The temperature dependence of the stability of Sac7d is in good agreement with chemical denaturation data presented previously (*47*). Denaturation by both urea and guanidine hydrochloride indicate a maximum in protein stability near room temperature. Analysis of the denaturation data with a linear extrapolation model (and including the T_m and $\Delta H(T_m)$ determined by DSC) indicated a ΔC_P of 881 (±60) cal/deg·mol, while a denaturant binding model gave a value of 709 (±118) cal/deg·mol. The χ^2 of the fits could not justify the preference for one value over the other. The stability of Sso7d described here is in qualitative agreement with two earlier thermodynamic studies of this protein. Knapp et al. (*49*) obtained similar values of ΔH of unfolding as a function of pH (down to 2.5), but the data were analyzed in the conventional manner. Graziano et al. (*67*) considered the effects of linkage of two carboxyl ionizations, but not chloride binding since no data were collected below pH 2.

It is not obvious what other differences between Sac7d and Sso7d (Figure 1) may be responsible for the remaining difference in stability between V30I and Sso7d (a vertical displacement of the stability curve by about 0.4 kcal/mol (Figure 8)). The Thr-to-Ile substitution at position 17 occurs in a partially solvent exposed crevice between a 3_{10} helix and the C-terminal α-helix, and is a likely candidate. Eight of the other differences are conservative surface substitutions which increase the charge on the protein by +2. The remaining include increasing the length of the loop between D35 and T40 with insertion of a glycine (possibly increasing flexibility), and deletion of three residues from the exposed C-terminal α-helix (possibly decreasing flexibility). Some of these substitutions are not those commonly expected to enhance the stability of thermophile proteins. For example, increased stability has been correlated with reduced loop length (*86*). In addition, increased thermostability has been shown to correlate with conversion of polar uncharged to charged residues, e.g., Gln to Glu (*21*), opposite to that observed here at positions 14, 56, and 64. Whether or not any of these affect the stability of the proteins remains to be demonstrated.

In summary, the data presented here on Sac7d and Sso7d indicate that van der Waals interactions are less important in defining the stability of the proteins (at least in the vicinity of residue 30) than in other proteins studied to date. A significant portion of the difference in stabilities of these proteins can be attributed to differences in hydrophobicity of the core, which is consistent with the minor differences in core structures of the two proteins (Figure 2). This has permitted an experimental demonstration of the temperature dependence of the hydrophobic effect in a protein. An

increase in the strength of salt bridges with temperature has been recently argued to be important in stabilizing thermophile proteins at in vivo growth temperatures (*87*). Experimental documentation of the magnitude of the temperature dependence of the contribution of a single salt bridge to the folding free energy of a protein is not available, but calculations indicate that the stabilization of a salt bridge should increase by about 0.8 kcal/mol with an increase in temperature of 85 °C (*87*). The increased benefit of core hydrophobicity with temperature is comparable (i.e., 0.7 kcal/methylene enhanced stability in going from 0 to 85 °C).

SUPPORTING INFORMATION AVAILABLE

Tables of analysis of accuracy and precision of fitted parameters in a global linkage analysis of simulated Sac7d test data (Table S1) and simulated Sso7d stability data (Table S2); and accuracy of unfolding free energies for Sac7d as a function of temperature, pH, and salt concentration obtained from a global linkage analysis of synthetic DSC and CD spectroscopic data (Table S3). Figures of effect of the cavity-filling V30I mutation in Sac7d and the cavity-creating mutation I30V in Sso7d on protein thermal stability monitored by DSC (Figure S1); overlay of ^{1}H,^{15}N HSQC spectra of Sso7d and the I30V mutant (Figure S2); and cross-sections through free energy surfaces for Sac7d, V30I, I30V, and Sso7d (Figure S3). This material is available free of charge via the Internet at http://pubs.acs.org.

REFERENCES

1. Chan, M. K., Mukund, S., Kletzin, A., Adams, M. W. W., and Rees, D. (1995) Structure of a hyperthermophilic tungsopterin enzyme, aldehyde ferredoxin oxidoreductase. *Science 267*, 1463−9.
2. Russell, R. J., Ferguson, J. M., Hough, D. W., Danson, M. J., and Taylor, G. L. (1997) The crystal structure of citrate synthase from the hyperthermophilic archaeon *Pyrococcus furiosu*s at 1.9 Å resolution. *Biochemistry 36*, 9983−94.
3. Delboni, L. F., Mande, S. C., Rentier-Delrue, F., Mainfroid, V., Turley, S., Vellieux, F. M., Martial, J. A., and Hol, W. G. (1995) Crystal structure of recombinant triosephosphate isomerase from *Bacillus stearothermophilus*. An analysis of potential thermostability factors in six isomerases with known three-dimensional structures points to the importance of hydrophobic interactions. *Protein Sci. 4*, 2594−604.
4. Russell, R. J., and Taylor, G. L. (1995) Engineering thermostability: lessons from thermophilic proteins. *Curr. Opin. Biotechnol. 6*, 370−4.
5. DeDecker, B., O'Brien, R., Fleming, P., Geiger, J., Jackson, S., and Sigler, P. (1996) The crystal structure of a hyperthermophile archael TATA-box binding protein. *J. Mol. Biol. 264*, 1072−84.
6. Querol, E., Perez-Pons, J. A., and Mozo-Villaries, A. (1996) Analysis of protein conformational characteristics related to thermostability. *Protein Eng. 9*, 265−71.
7. Knapp, S., de Vos, W. M., Rice, D., and Ladenstein, R. (1997) Crystal structure of glutamate dehydrogenase from the hyperthermophilic eubacterium *Thermotoga maritima* at 3.0 Å resolution. *J. Mol. Biol. 267*, 916−32.
8. Hopfner, K. P., Eichinger, A., Engh, R. A., Laue, F., Ankenbauer, W., Huber, R., and Angerer, B. (1999) Crystal structure of a thermostable type B DNA polymerase from *Thermococcus gorgonarius*. *Proc. Natl. Acad. Sci. U.S.A. 96*, 3600−5.
9. Vetriani, C., Maeder, D. L., Tolliday, N., Yip, K. S., Stillman, T. J., Britton, K. L., Rice, D. W., Klump, H. H., and Robb, F. T. (1998) Protein thermostability above 100 °C: a key role for ionic interactions. *Proc. Natl. Acad. Sci. U.S.A. 95*, 12300−5.
10. Charron, C., Talfournier, F., Isupov, M. N., Littlechild, J. A., Branlant, G., Vitoux, B., and Aubry, A. (2000) The crystal structure of D-glyceraldehyde-3-phosphate dehydrogenase from the hyperthermophilic archaeon *Methanothermus fervidus* in the presence of $NADP^{+}$ at 2.1 Å resolution. *J. Mol. Biol. 297*, 481−500.
11. Auerbach, G., Ostendorp, R., Prade, L., Korndorfer, I., Dams, T., Huber, R., and Jaenicke, R. (1998) Lactate dehydrogenase from the hyperthermophilic bacterium *Thermotoga maritima*: the crystal structure at 2.1 Å resolution reveals strategies for intrinsic protein stabilization. *Structure 6*, 769−81.
12. Li, W.-T., Grayling, R., Sandman, K., Edmondson, S., Shriver, J. W., and Reeve, J. N. (1998) Thermodynamic stability of archaeal histones, *Biochemistry 37*, 10563−72.
13. Li, W. T., Shriver, J. W., and Reeve, J. N. (2000) Mutational analysis of differences in thermostability between histones from mesophilic and hyperthermophilic archaea. *J. Bacteriol. 182*, 812−7.
14. Ikai, A. (1980) Thermostability and aliphatic index of globular proteins. *J. Biochem. 88*, 1895−8.
15. Britton, K. L., Baker, P. J., Borges, K. M. M., Engel, P. C., Pasquo, A., Rice, D. W., Robb, F. T., Scandurra, R., Stillman, T., and Yip, K. S. P. (1995) Insights into thermal stability from a comparison of the glutamate dehydrogenases from *Pyrococcus furiosus* and *Thermococcus litoralis*. *Eur. J. Biochem. 229*, 688−95.
16. Yip, K. S. P., Stillman, T. J., Britton, K. L., Artymiuk, P. J., Baker, P. J., Sekelnikova, S. E., Engel, P. C., Pasquo, A., Chiaraluce, R., Consalvi, V., Scandurra, R., and Rice, D. W. (1995) The Structure of *Pyrococcus furiosus* glutamate dehydrogenase reveals a key role for ion pair networks in maintaining enzyme stability at extreme temperatures. *Structure 3*, 1147−58.
17. Tanner, J. J., Hecht, R. M., and Krause, K. L. (1996) Determinants of enzyme thermostability observed in the molecular structure of *Thermus aquaticus* D-glyceraldehyde-3-phosphate dehydrogenase at 25 Å Resolution. *Biochemistry 35*, 2597−609.
18. Knapp, S., Kardinahl, S., Hellgren, N., Tibbelin, G., Schafer, G., and Ladenstein, R. (1999) Refined crystal structure of a superoxide dismutase from the hyperthermophilic archaeon *Sulfolobus acidocaldarius* at 2.2 Å resolution. *J. Mol. Biol. 285*, 689−702.
19. Vogt, G., and Argos, P. (1997) Protein thermal stability: hydrogen bonds or internal packing? *Fold Des. 2*, S40−6.
20. Karshikoff, A., and Ladenstein, R. (1998) Proteins from thermophilic and mesophilic organisms essentially do not differ in packing. *Protein Eng. 11*, 867−72.
21. Haney, P. J., Badger, J. H., Buldak, G. L., Reich, C. I., Woese, C. R., and Olsen, G. J. (1999) Thermal adaptation analyzed by comparison of protein sequences from mesophilic and extremely thermophilic *Methanococcus* species. *Proc. Natl. Acad. Sci. U.S.A. 96*, 3578−83.
22. Szilagyi, A., and Zavodszky, P. (2000) Structural differences between mesophilic, moderately thermophilic and extremely thermophilic protein subunits: results of a comprehensive survey. *Structure Fold Des. 8*, 493−504.
23. Rees, D. C., and Robertson, A. D. (2001) Some thermodynamic implications for the thermostability of proteins. *Protein Sci. 10*, 1187−94.
24. Kumar, S., Tsai, C. J., and Nussinov, R. (2001) Thermodynamic differences among homologous thermophilic and mesophilic proteins. *Biochemistry 40*, 14152−65.
25. Lim, W. A., and Sauer, R. T. (1989) Alternative packing arrangements in the hydrophobic core of lambda repressor. *Nature 339*, 31−6.
26. Dill, K. A. (1990) Dominant forces in protein folding. *Biochemistry 29*, 7133−55.
27. Kauzmann, W. (1955) Some factors in the interpretation of protein denaturation. *Adv. Protein Chem. 14*, 1−63.
28. Richards, F. M., and Lim, W. A. (1993) An analysis of packing in the protein folding problem. *Q. Rev. Biophys. 26*, 423−98.
29. Hubbard, S. J., and Argos, P. (1995) Evidence on close packing and cavities in proteins. *Curr. Opin. Biotechnol. 6*, 375−81.
30. Makhatadze, G., and Privalov, P. L. (1995) Energetics of Protein Structure. *Adv. Prot. Chem. 47*, 308−425.
31. Lee, B., and Vasmatzis, G. (1997) Stabilization of protein structures, *Curr. Opin. Biotechnol. 8*, 423−8.
32. Holder, J. B., Bennett, A. F., Chen, J., Spencer, D. S., Byrne, M. P., and Stites, W. E. (2001) Energetics of side chain packing in staphylococcal nuclease assessed by exchange of valines, isoleucines, and leucines. *Biochemistry 40*, 13998−4003.
33. Karpusas, M., Baase, W. A., Matsumura, M., and Matthews, B. W. (1989) Hydrophobic packing in T4 lysozyme probed by cavity-filling mutants, *Proc. Natl. Acad. Sci. U.S.A. 86*, 8237−41.

34. Ishikawa, K., Nakamura, H., Morikawa, K., and Kanaya, S. (1993) Stabilization of *Escherichia coli* ribonuclease HI by cavity-filling mutations within a hydrophobic core. *Biochemistry 32*, 6171−8.
35. Morii, H., Uedaira, H., Ogata, K., Ishii, S., and Sarai, A. (1999) Shape and energetics of a cavity in c-Myb probed by natural and nonnatural amino acid mutations. *J. Mol. Biol. 292*, 909−20.
36. Chen, J., Lu, Z., Sakon, J., and Stites, W. E. (2000) Increasing the thermostability of *Staphylococcal* nuclease: implications for the origin of protein thermostability. *J. Mol. Biol. 303*, 125−30.
37. Xu, J., Baase, W. A., Baldwin, E., and Matthews, B. W. (1998) The response of T4 lysozyme to large-to-small substitutions within the core and its relation to the hydrophobic effect. *Protein Sci. 7*, 158−77.
38. Jackson, S. E., Moracci, M., elMasry, N., Johnson, C. M., and Fersht, A. R. (1993) Effect of cavity-creating mutations in the hydrophobic core of chymotrypsin inhibitor. *Biochemistry 32*, 11259−69.
39. Kellis, J., Nyberg, K., Sali, D., and Fersht, A. (1988) Contribution of hydrophobic interactions to protein stability. *Nature 333*, 784−6.
40. Kellis, J., Nyberg, K., and Fersht, A. (1989) Energetics of complementary side-chain packing in a protein hydrophobic core. *Biochemistry 28*, 4914−22.
41. Eriksson, A., Baase, W., Zhang, X.-J., Heinz, D., Blaber, M., Baldwin, E., and Matthews, B. (1993) Response of a protein structure to cavity-creating mutations and its relation to the hydrophobic effect. *Science 255*, 178−83.
42. Ratnaparkhi, G. S., and Varadarajan, R. (2000) Thermodynamic and structural studies of cavity formation in proteins suggest that loss of packing interactions rather than the hydrophobic effect dominates the observed energetics. *Biochemistry 39*, 12365−74.
43. Chen, J., and Stites, W. E. (2001) Packing is a key selection factor in the evolution of protein hydrophobic cores. *Biochemistry 40*, 15280−9.
44. Mendel, D., Ellman, J. A., Chang, Z., Veenstra, D. L., Kollman, P. A., and Schultz, P. G. (1992) Probing protein stability with unnatural amino acids. *Science 256*, 1798−802.
45. Loladze, V. V., Ermolenko, D. N., and Makhatadze, G. I. (2001) Heat capacity changes upon burial of polar and nonpolar groups in proteins. *Protein Sci. 10*, 1343−52.
46. Loladze, V. V., Ermolenko, D. N., and Makhatadze, G. I. (2002) Thermodynamic consequences of burial of polar and nonpolar amino acid residues in the protein interior. *J. Mol. Biol. 320*, 343−57.
47. McCrary, B. S., Edmondson, S. P., and Shriver, J. W. (1996) Hyperthermophile protein folding thermodynamics: Differential scanning calorimetry and chemical denaturation of Sac7d. *J. Mol. Biol. 264*, 784−805.
48. Edmondson, S. P., Qiu, L., and Shriver, J. W. (1995) Solution structure of the DNA-binding protein Sac7d from the hyperthermophile *Sulfolobus acidocaldarius*. *Biochemistry 34*, 13289−304.
49. Knapp, S., Karshikoff, A., Berndt, K. D., Christova, P., Atanasov, B., and Ladenstein, R. (1996) Thermal unfolding of the DNA-binding protein Sso7d from the hyperthermophile *Sulfolobus solfataricus*. *J. Mol. Biol. 264*, 1132−44.
50. McAfee, J., Edmondson, S., Datta, P., Shriver, J., and Gupta, R. (1995) Gene cloning, sequencing, expression, and characterization of the Sac7 DNA-binding proteins from the extremely thermophilic archaeon *Sulfolobus acidocaldarius*. *Biochemistry 34*, 10063−77.
51. Kay, L. E., Keifer, P., and Saarinen, T. (1992) Pure absorption gradient enhanced heteronuclear single quantum correlation spectroscopy with improved sensitivity. *J. Am. Chem. Soc. 114*, 10663−5.
52. Zhang, O., Kay, L. E., Olivier, J. P., and Forman-Kay, J. D. (1994) Backbone ^{1}H and ^{15}N resonance assignments of the N-terminal SH_3 domain of drk in folded and unfolded states using enhanced-sensitivity pulsed field gradient NMR techniques. *J. Biomol. NMR 4*, 845−58.
53. Markley, J. L., Bax, A., Arata, Y., Hilbers, C. W., Kaptein, R., Sykes, B. D., Wright, P. E., and Wuthrich, K. (1998) Recommendations for the presentation of NMR structures of proteins and nucleic acids. *J. Mol. Biol. 280*, 933−52.
54. Bedell, J. L., McCrary, B. S., Edmondson, S. P., and Shriver, J. W. (2000) The acid-induced folded state of Sac7d is the native state. *Protein Sci. 9*, 1878−88.
55. McCrary, B. S., Bedell, J., Edmondson, S. P., and Shriver, J. W. (1998) Linkage of protonation and anion binding to the folding of Sac7d. *J. Mol. Biol. 276*, 203−24.
56. Krueger, J. K., McCrary, B. S., Wang, A. H., Shriver, J. W., Trewhella, J., and Edmondson, S. P. (1999) The solution structure of the Sac7d/DNA complex: a small-angle X-ray scattering study. *Biochemistry 38*, 10247−55.
57. Pitzer, K. S. (1973) Thermodynamics of electrolytes. I. Theoretical basis and general equations. *J. Phys. Chem. 77*, 268−77.
58. Bevington, P. R., and Robinson, D. K. (1992) *Data Reduction and Error Analysis for the Physical Sciences*, McGraw-Hill, New York.
59. Press, W., Flannery, B., Teukolsky, S., and Vetterling, W. (1989) *Numerical Recipes: The Art of Scientific Computing (Fortran Version)*, Cambridge University Press, Cambridge.
60. Pace, C. N., and Laurents, D. (1989) A new method for determining the heat capacity change for protein folding. *Biochemistry 28*, 2520−5.
61. Pace, C. N., Hebert, E. J., Shaw, K. L., Schell, D., Both, V., Krajcikova, D., Sevcik, J., Wilson, K. S., Dauter, Z., Hartley, R. W., and Grimsley, G. R. (1998) Conformational stability and thermodynamics of folding of ribonucleases Sa, Sa2 and Sa3. *J. Mol. Biol. 279*, 271−86.
62. Pace, C. N., Grimsley, G. R., Thomas, S. T., and Makhatadze, G. I. (1999) Heat capacity change for ribonuclease A folding. *Protein Sci. 8*, 1500−4.
63. Robertson, A. D., and Murphy, K. P. (1997) Protein structure and the energetics of protein stability. *Chem. Rev. 97*, 1251−67.
64. Baumann, H., Knapp, S., Lundbach, T., Ladenstein, R., and Hard, T. (1994) Solution structure and DNA-binding properties of a thermostable protein from the archaeon *Sulfolobus solfataricus*. *Nat. Struct. Biol. 1*, 808−19.
65. Gao, Y., Su, S., Robinson, H., Padmanabhan, S., Lim, L., McCrary, B., Edmondson, S., Shriver, J., and Wang, A. (1998) The crystal structure of the hyperthermophile chromosomal protein Sso7d bound to DNA. *Nat. Struct. Biol. 5*, 782−6.
66. Lewis, G. N., Randall, M., Pitzer, K. S., and Brewer, L. (1961) *Thermodynamics*, McGraw-Hill, New York.
67. Graziano, G., Catanzano, F., and Nappaaaaa, M. (1999) The linkage of proton binding to the thermal unfolding of Sso7d from the hyperthermophile archaebacterium *Sulfolobus solfataricus*. *Int. J. Biol. Macromol. 26*, 45−53.
68. Steif, C., Hinz, H. J., and Cesareni, G. (1995) Effects of cavity-creating mutations on conformational stability and structure of the dimeric 4-alpha-helical protein ROP: thermal unfolding studies. *Proteins 23*, 83−96.
69. Taniuchi, H., Shi, Y., San Miguel, G. I., Ferretti, J. A., Mack, J. W., Fisher, A., Shah, M., Schechter, A. N., and Shiloach, J. (2001) A study of the influence of the hydrophobic core residues of yeast iso-2-cytochrome *c* on phosphate binding: a probe of the hydrophobic core-surface charge interactions. *J. Protein Chem. 20*, 203−15.
70. Pace, C. N. (1992) Contribution of the hydrophobic effect to globular protein stability. *J. Mol. Biol. 226*, 29−35.
71. Fauchere, J.-L., and Pliska, V. (1983) Hydrophobic parameters π of amino acid side-chains from the partitioning of *N*-acetyl-amino acid amides. *Eur. J. Med. Chem.-Chim. Ther. 18*, 369−375.
72. Wimley, W. C., Creamer, T. P., and White, S. H. (1996) Solvation energies of amino acid side chains and backbone in a family of host−guest pentapeptides. *Biochemistry 35*, 5109−24.
73. Lee, K. H., Xie, D., Freire, E., and Amzel, L. M. (1994) Estimation of changes in side chain configurational entropy in binding and folding: general methods and application to helix formation. *Proteins 20*, 68−84.
74. Sturtevant, J. (1977) Heat capacity and entropy changes in processes involving proteins, *Proc. Natl. Acad. Sci. U.S.A. 74*, 2236−40.
75. Tanford, C. (1980) *The Hydrophobic Effect: Formation of Micelles and Biological Membranes*, 2nd ed., John Wiley and Sons, New York.
76. Ross, P., and Subramanian, S. (1981) Thermodynamics of protein association reactions: Forces contributing to stability. *Biochemistry 20*, 3096−102.
77. Makhatadze, G. I., and Privalov, P. L. (1990) Heat capacity of proteins. I. Partial molar heat capacity of individual amino acid residues in aqueous solution: hydration effect. *J. Mol. Biol. 213*, 375−84.
78. Murphy, K. P., and Freire, E. (1992) Thermodynamics of structural stability and cooperative folding behavior in proteins. *Adv. Prot. Chem. 43*, 313−61.

79. Spolar, R. S., Livingstone, J. R., and Record, M. T., Jr. (1992) Use of liquid hydrocarbon and amide transfer data to estimate contributions to thermodynamic functions of protein folding from the removal of nonpolar and polar surface from water. *Biochemistry 31*, 3947−55.
80. Myers, J., Pace, C. N., and Scholtz, J. M. (1995) Denaturant *m* values and heat capacity changes: Relation to changes in accessible surface areas of protein unfolding. *Protein Sci. 4*, 2138−48.
81. Jelesarov, I., and Bosshard, H. R. (1996) Thermodynamic characterization of the coupled folding and association of heterodimeric coiled coils (leucine zippers). *J. Mol. Biol. 263*, 344−58.
82. Becktel, W., and Schellman, J. (1987) Protein stability curves. *Biopolymers 26*, 1859−77.
83. Durr, E., and Jelesarov, I. (2000) Thermodynamic analysis of cavity creating mutations in an engineered leucine zipper and energetics of glycerol-induced coiled coil stabilization. *Biochemistry 39*, 4472−82.
84. Thomas, S. T., and Makhatadze, G. I. (2000) Contribution of the 30/36 hydrophobic contact at the C-terminus of the alpha-helix to the stability of the ubiquitin molecule. *Biochemistry 39*, 10275−83.
85. Robinson, H., Gao, Y. G., McCrary, B. S., Edmondson, S. P., Shriver, J. W., and Wang, A. H. (1998) The hyperthermophile chromosomal protein Sac7d sharply kinks DNA. *Nature 392*, 202−5.
86. Vieille, C., and Zeikus, J. G. (1996) Thermozymes: identifying molecular determinants of protein structural and functional stability. *TIBTECH 14*, 183−90.
87. Elcock, A. H. (1998) The stability of salt bridges at high temperatures: implications for hyperthermophilic proteins. *J. Mol. Biol. 284*, 489−502.
88. Kimura, M., Kimura, J., Davie, P., Reinhardt, R., and Dijk, J. (1984) The amino acid sequence of a small DNA binding protein form the archaebacterium *Sulfolobus solfataricus*. *FEBS Lett. 176*, 176−8.
89. Choli, T., Henning, P., Wittmann-Liebold, B., and Reinhardt, R. (1988) Isolation, characterization, and microsequence analysis of a small basic methylated DNA-binding protein from the Archaebacterium, *Sulfolobus solfataricus*. *Biochim. Biophys. Acta 950*, 193−203.

BI0358263